Environmental Science & Technology

Article

pubs.acs.org/est

Secondary Organic Aerosol Formation from in-Use Motor Vehicle Emissions Using a Potential Aerosol Mass Reactor

Daniel S. Tkacik,[†,¶] Andrew T. Lambe,[‡] Shantanu Jathar,[§] Xiang Li,[¶,∥] Albert A. Presto,[¶,∥] Yunliang Zhao,[¶,∥] Donald Blake,[⊥] Simone Meinardi,[⊥] John T. Jayne,[‡] Philip L. Croteau,[‡] and Allen L. Robinson*[,¶,∥]

[†]Department of Civil and Environmental Engineering, Carnegie Mellon University, Pittsburgh, Pennsylvania 15213, United States

[¶]Center for Atmospheric Particle Studies, Carnegie Mellon University, Pittsburgh, Pennsylvania 15213, United States

[‡]Aerodyne Research, Inc., Billerica, Massachusetts 01821, United States,

[§]Civil and Environmental Engineering, University of California, Davis, Davis, California 95616, United States

[∥]Mechanical Engineering, Carnegie Mellon University, Pittsburgh, Pennsylvania 15213, United States

[⊥]Department of Chemistry, University of California, Irvine, Irvine, California 92697-2025, United States

Supporting Information

ABSTRACT: Secondary organic aerosol (SOA) formation from in-use vehicle emissions was investigated using a potential aerosol mass (PAM) flow reactor deployed in a highway tunnel in Pittsburgh, Pennsylvania. Experiments consisted of passing exhaust-dominated tunnel air through a PAM reactor over integrated hydroxyl radical (OH) exposures ranging from ~0.3 to 9.3 days of equivalent atmospheric oxidation. Experiments were performed during heavy traffic periods when the fleet was at least 80% light-duty gasoline vehicles on a fuel-consumption basis. The peak SOA production occurred after 2−3 days of equivalent atmospheric oxidation. Additional OH exposure decreased the SOA production presumably due to a shift from functionalization to fragmentation dominated reaction mechanisms. Photo-oxidation also produced substantial ammonium nitrate, often exceeding the mass of SOA. Analysis with an SOA model highlight that unspeciated organics (i.e., unresolved complex mixture) are a very important class of precursors and that multigenerational processing of both gases and particles is important at longer time scales. The chemical evolution of the organic aerosol inside the PAM reactor appears to be similar to that observed in the atmosphere. The mass spectrum of the unoxidized primary organic aerosol closely resembles ambient hydrocarbon-like organic aerosol (HOA). After aging the exhaust equivalent to a few hours of atmospheric oxidation, the organic aerosol most closely resembles semivolatile oxygenated organic aerosol (SV-OOA) and then low-volatility organic aerosol (LV-OOA) at higher OH exposures. Scaling the data suggests that mobile sources contribute ~2.9 ± 1.6 Tg SOA yr^{-1} in the United States, which is a factor of 6 greater than all mobile source particulate matter emissions reported by the National Emissions Inventory. This highlights the important contribution of SOA formation from vehicle exhaust to ambient particulate matter concentrations in urban areas.

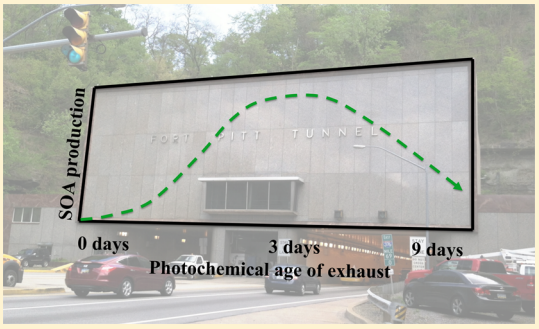

1. INTRODUCTION

Motor vehicle emissions are an important source of particulate matter (PM) in urban areas,[1,2] adversely affecting public health and influencing climate.[3,4] Vehicles directly emit PM, which is mainly comprised of black carbon (BC) and primary organic aerosols (POA). Vehicle exhaust also forms "secondary" PM through the oxidation of gas-phase organic emissions to form secondary organic aerosol (SOA) and the oxidation of oxides of nitrogen to form nitrate aerosol.[5−8] Substantial SOA production occurs downwind of urban areas, but models based on laboratory-measured SOA yields fail to explain these observations.[9−12] A key question is: what role do vehicle emissions play in ambient SOA production? Addressing this question requires investigating SOA formation from vehicles that are representative of actual traffic fleets and driving conditions.

Recent studies have investigated SOA formation from dilute vehicle emissions using smog chambers.[6,8,13−15] In these studies, emissions from individual vehicles were photo-oxidized via UV-irradiation in a smog chamber under various conditions. With the exception of diesel vehicles equipped with particulate filters and oxidation catalysts, all vehicle emissions formed substantial amounts of SOA with photo-oxidation, and, in most

Received: May 6, 2014
Revised: August 11, 2014
Accepted: September 4, 2014
Published: September 4, 2014

cases, the amount of SOA exceeded POA after aging the emissions for less than the equivalent of 1 day at typical atmospheric oxidant concentrations. However, since vehicle exhaust can reside in the atmosphere for up to a week or more, chamber studies may not characterize the full SOA production potential associated with multiple generations of oxidation.[16] In addition, smog chamber experiments have only been performed with exhaust from a small number of vehicles that may or may not be representative of actual in-use vehicle fleets. Many tunnel studies have characterized primary emissions from large fleets of motor vehicles,[17−19] but to date, no tunnel studies have quantified SOA formation from motor vehicle emissions.

In this study, we investigated SOA formation from a large fleet of on-road vehicles inside the Fort Pitt Tunnel on Interstate-376 in Pittsburgh, Pennsylvania. The tunnel air was oxidized with the hydroxyl radical (OH) inside a potential aerosol mass (PAM) reactor[20] over exposures ranging from several hours to several days of typical atmospheric oxidation. The data were analyzed to quantify the SOA production and to characterize SOA composition as a function of oxidant exposure. The data are compared to ambient measurements and scaled to provide an estimate of the contribution of in-use vehicles to SOA formation on the national level.

2. EXPERIMENTAL METHODS

2.1. Sampling Setup in the Fort Pitt Tunnel. Experiments were conducted during a two-week period in May 2013 in the two-lane westbound bore of the Fort Pitt Tunnel on Interstate-376 in Pittsburgh, Pennsylvania. The bore is 8.5 m wide, 4.1 m tall, and 1.1 km long with a 2.5% uphill grade so the vehicles were operating under load. The tunnel is mechanically ventilated through ducts situated in the tunnel ceiling and by airflow created by traffic motion.

Supporting Information (SI) Figure S1 shows time series of weekday traffic flow rate, vehicle speed, and fraction of light-duty vehicles (LDVs) during the study period. Traffic data were collected using a Remote Traffic Microwave Sensor operated by the Pennsylvania Department of Transportation (PennDOT). An average of 61 450 (±2600 standard deviation) vehicles passed through the tunnel per day, with hourly traffic volumes peaking between 3500−4000 vehicles per hour during morning and evening rush hours. Between 90 and 96% of the traffic fleet during the experimental periods consisted of LDVs, which in the United States, are mainly gasoline-fueled. Vehicles per hour and fraction of LDVs were fairly steady—neither metric changed more than 5% during a single experiment. Assuming an average fuel efficiency for new and used LDVs and heavy-duty vehicles (HDVs) of 21 and 6 miles per gallon, respectively,[21] 80−85% of the fuel consumption during measurement periods was by LDVs. Pittsburgh city bus routes do not pass through the tunnel.

Figure S2 in the SI shows the sampling setup in the tunnel. The sample inlets were inserted through a sealed ventilation slit in the tunnel ceiling approximately 50 m from the tunnel exit. Ventilation slits upstream and downstream of the sample inlet were blocked to reduce dilution of emissions near the sampling location. Gas and particle sampling lines were 22 m long due to constraints on where the instrumentation could be deployed. Gas sampling lines were 0.5 in diameter Teflon tubing, and particle sampling lines were 0.325 in diameter copper tubing. The Reynolds number for the particle sampling line was <2000, indicating laminar flow.

2.2. OH Oxidation of Vehicle Exhaust. Tunnel air was sampled into a potential aerosol mass (PAM) flow reactor[14,18−20] where it was oxidized by exposure to hydroxyl (OH) radicals. The average residence time in the PAM flow tube was approximately 100 s. The PAM reactor was placed at the beginning of the sampling line, ∼ 10 cm downstream of the sample inlet to minimize losses of SOA precursors. A three-way valve was used to alternately sample tunnel air from the PAM reactor or a bypass line.

Four UV mercury lamps (BHK Inc.) were used to initiate photochemistry inside the PAM reactor. The lamps emit light at 185 and 254 nm. At 185 nm, O_2 is photolyzed to produce O_3 and H_2O is photolyzed to produce OH and HO_2. At 254 nm, O_3 is photolyzed to produce $O(^1D)$, which reacts with H_2O to produce OH. O_3 levels inside the PAM reactor (0−20 ppm) are not expected to significantly influence SOA formation because SOA precursors present in vehicle emissions are dominated by aromatics and saturated hydrocarbons[22] that are unreactive toward O_3. High O_3 levels may suppress reactions of nitric oxide (NO) with organic peroxy radicals (RO_2) formed from OH oxidation of vehicle emissions, but the effect on SOA formation is probably minor.[23]

OH concentrations were systematically varied by changing the UV lamp voltages between 0 and 110 V. The OH exposure, which is the product of OH concentration and average residence time in the PAM reactor, was determined by measuring the decay of SO_2 as a function of lamp intensity in offline calibrations. NO_x levels in the tunnel were high (400−1300 ppb); therefore, NO_x was a large OH sink. To account for this sink, the OH calibrations were performed with a range of NO concentrations representative of tunnel conditions, where a known amount of NO was added to the PAM reactor along with SO_2 and the corresponding reduction in OH exposure was measured. SI Figures S4−S6 show the reduction in OH exposure at low, midrange, and high lamp intensity respectively in the PAM reactor as a function of [NO]. From these data we calculated the reduced OH exposure for tunnel measurements as a function of lamp intensity at the mean tunnel NO mixing ratio (459 ppb). OH exposures ranged from 7.4×10^{10} to 2.4×10^{12} molecules cm^{-3} s or approximately 0.3−9.3 days of equivalent photochemical aging at a typical urban OH concentration of 3×10^6 molecules cm^{-3}.[24] VOCs may also reduce the OH exposure in the PAM reactor, but this reduction was likely much smaller than that due to NO_x since VOC levels were much lower than NO_x levels. Thus, the estimated OH exposures represent an upper limit of the actual exposures inside the PAM reactor during tunnel measurements.

2.3. Instrumentation. Nonrefractory PM_1 mass was measured using an Aerodyne Aerosol Chemical Speciation Monitor (ACSM),[25] which quantifies concentrations of organic, nitrate, ammonium, sulfate, and chloride species at unit mass resolution. The ACSM was operated at 1 min resolution in the tunnel, which is significantly higher than the more typical 15−30 min resolution, because of the relatively high PM concentrations. ACSM data were corrected for collection efficiency (CE), which was estimated by comparing ACSM mass concentrations to concurrent scanning-mobility particle sizer (SMPS, TSI 3080) mass concentrations assuming PM density weighted by the proportions of major chemical constituents (i.e., organics = 1.0 g cm^{-3}, ammonium nitrate = 1.73 g cm^{-3}). The range of CE applied to the aged aerosol was 0.5−0.7, depending on extent of oxidation, consistent with the

decrease in CE with organic aerosol (OA) aging reported in other studies.[26−28] Black carbon (BC) mass concentrations were measured using an Aethalometer (Magee Scientific model AE-31).

Gas-phase measurements included carbon dioxide (CO_2, Licor Biosciences model LI-820), carbon monoxide (CO, API model 300), NO_x (Teledyne model 200 EU), and O_3 (API model 400A). For three experiments, samples of tunnel air upstream of the PAM reactor were collected onto Tenax TA sorbent tubes. These samples were analyzed off-line using thermal desorption system (TDS3, Gerstel Inc.) coupled with a gas chromatograph (GC) equipped with a mass-selective detector (Agilent 6890 and 5975) to quantify concentrations of intermediate volatility organic compounds (IVOCs; see SI).[29] During select experiments, whole air samples (WAS) were also collected upstream of the PAM reactor using 2 L evacuated stainless steel canisters equipped with stainless steel bellows valves. The WAS were analyzed to quantify concentrations of 49 volatile organic compounds (VOC)—C_2 − C_{10} hydrocarbons, including alkanes, alkenes, and single-ring aromatics using a GC equipped with flame-ionization and mass-selective detectors.[30]

2.4. Background Pollutant Concentrations. The pollutant data measured inside the tunnel were corrected for urban-background pollutant concentrations, which were a factor of ∼3−30 times lower than concentrations inside the tunnel. SI Table S1 lists typical tunnel and background concentrations of OA, NO_x, CO, and CO_2.

Background concentrations of $PM_{2.5}$ and CO were measured at an urban background site operated by the Allegheny County Health Department located in the Lawrenceville neighborhood of Pittsburgh, approximately 6 km northeast of the tunnel site. Previous studies have demonstrated that this site provides a good estimate of urban background pollutant levels.[31] To estimate background organic aerosol (OA), we used the average chemical speciation of $PM_{2.5}$ from the Pittsburgh Air Quality Study.[32] POA concentrations in the tunnel were typically 2−5 times higher than the estimated background OA concentrations, and SOA concentrations in this study were at least an order of magnitude higher than background OA concentrations. Background concentrations of CO_2 were assumed to be 400 ppm, which was the minimum CO_2 level measured in the tunnel when traffic levels were very low. The CO_2 level in Pittsburgh may fluctuate by ±10 ppm, which is only ∼5% of the smallest background-corrected CO_2 level measured in the tunnel.

2.5. Calculating SOA Production. SOA production was quantified on a fuel-consumption basis using a carbon balance:

$$\text{SOA production, mg(kg} - \text{fuel)}^{-1} = \frac{\text{OA}_{\text{PAM}} - \text{OA}_{\text{bypass}}}{\text{total C}} \times \text{C}_\text{f} \quad (1)$$

where OA_{PAM} is the OA concentration (mg m^{-3}) measured downstream of the PAM reactor, OA_{bypass} is the OA concentration (mg m^{-3}) in the bypass line. Total C is the total carbon concentration, defined by

$$\text{total C} = \left(\frac{\Delta \text{CO}_2}{\text{MW}_{\text{CO}_2}} + \frac{\Delta \text{CO}}{\text{MW}_{\text{CO}}} + \frac{\Delta \text{VOC}}{\text{MW}_{\text{VOC}}} \right) \times \text{MW}_\text{C} \quad (2)$$

where ΔCO_2, ΔCO, and ΔVOC are the background-corrected CO_2, CO, and VOC concentrations in the tunnel (mg m^{-3}), respectively, and MW_{CO2}, MW_{CO}, MW_{VOC}, and MW_C are the molecular weights of CO_2, CO, VOC, and carbon (mg mol^{-1}), respectively, and C_f is the carbon content of fuel. For this study, we assumed a carbon content of gasoline of 0.86 (kg-carbon kg-$fuel^{-1}$).[33] The carbon contributions from CO and VOCs were typically <1% and ≪1%, respectively.

3. RESULTS AND DISCUSSION

3.1. Primary Emissions. Primary emissions data calculated from the unoxidized tunnel air are listed in SI Table S2. VOC, BC, NO_x, and POA emissions measured in the tunnel fall within the range of gasoline and diesel emissions reported in previous studies.[33,34] Assuming gasoline/diesel fuel consumption fractions indicated by traffic data and reported vehicle class fractions (see SI), primary emission factors measured in the tunnel are within ±5−40% of expected emissions based on emission factors reported in previous vehicle emissions studies.[5,35]

3.2. Secondary PM Production. Figure 1 shows time series of data from a typical PAM reactor experiment. The

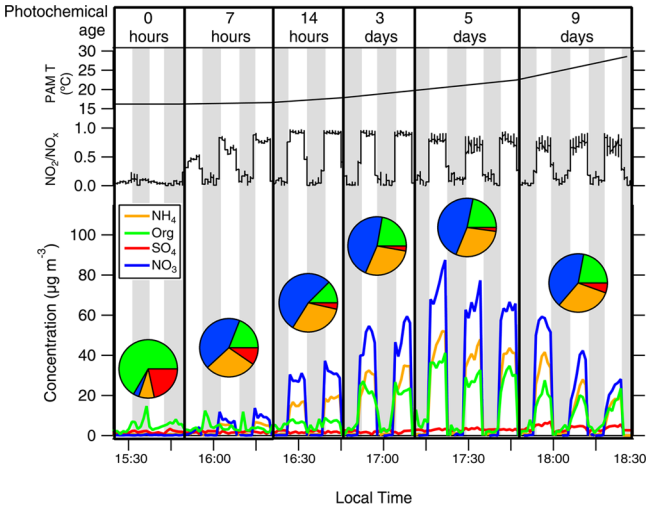

Figure 1. Time series of ammonium, sulfate, organics, and nitrate measured by the ACSM. Shaded periods are when the tunnel air bypassed the PAM reactor. Equivalent atmospheric oxidation (i.e., "1 day" at [OH] = 3 × 10^6 cm^{-3}) is shown at the top of the plot. This experiment was conducted on May 13, 2013, and is representative of other experiments.

shaded regions are periods when tunnel air bypassed the PAM reactor and was not subjected to OH oxidation. The nonshaded regions correspond to periods when the tunnel air was processed inside the PAM reactor at a specific OH exposure, indicated on the top axis in units of "OH days," calculated assuming [OH] = 3 × 10^6 molecules cm^{-3}.

During bypass periods, Figure 1 indicates that ACSM-measured nonrefractory PM mass loadings varied between 6−12 μg m^{-3} (∼60% organic, 25−30% sulfate, 10−15% ammonium and nitrate) and that NO_x was present mostly in the form of NO (NO_2/NO_x < 5%). When tunnel air was oxidized inside the PAM reactor (nonshaded periods in Figure 1), PM mass loadings increased significantly. SOA concentrations (defined as the difference between the OA measured downstream of the PAM reactor and the bypass line) ranged from 5 and 50 μg m^{-3} depending on OH exposure. SOA formation from background air was assessed and found to be

dx.doi.org/10.1021/es502239v | Environ. Sci. Technol. 2014, 48, 11235−11242

negligible (see SI). Therefore, the SOA production shown in Figure 1 is due to vehicle exhaust. There was also significant formation of particle-phase ammonium nitrate due to the oxidation of NO emissions to HNO_3 inside the PAM reactor which was then neutralized by the NH_3 emitted by gasoline vehicles.[17,36−38] The ammonium nitrate production exceeded that of SOA by about a factor of 2, underscoring the significant contribution of motor vehicle emissions to secondary inorganic aerosol formation. Gordon et al.[5] also observed significant ammonium nitrate formation in smog chamber studies with gasoline vehicles. The conversion efficiency of NO_x to nitrate inside the PAM reactor ranged from 7−25% at OH levels at ∼3 OH days, which is consistent with NO_x conversion efficiencies observed in the atmosphere.[39]

Figure 1 indicates that the nitrate levels also decreased at high OH exposure. We attribute this decrease to evaporation due to a ∼ 10 °C temperature rise at the highest UV lamp intensity. This temperature increase likely has minimal effect on the gas-particle partition of the highly oxidized organic aerosol formed at high OH exposures.

Figure 2 shows a box-and-whisker plot that summarizes the SOA data as a function of OH exposure. The top axis shows the equivalent atmospheric photochemical age in OH days assuming [OH] = 3 × 10^6 molecules cm^{-3}. The peak SOA production (∼350 mg kg-$fuel^{-1}$) was measured at an OH exposure of 6.9 × 10^{11} molecules cm^{-3} s or 2.7 OH days. The SOA production then decreased with additional OH exposure. This trend is qualitatively similar to laboratory SOA data from photo-oxidation of large alkanes.[14] At lower OH exposures, functionalization-dominated reaction mechanisms produce low vapor pressure gas-phase species to produce SOA. At higher OH exposures, continued oxidation fragments carbon−carbon bonds and forms higher vapor pressure products that reduce SOA levels. This transition from functionalization- to fragmentation-dominated reaction mechanisms was observed in all PAM reactor oxidation experiments performed in the tunnel.

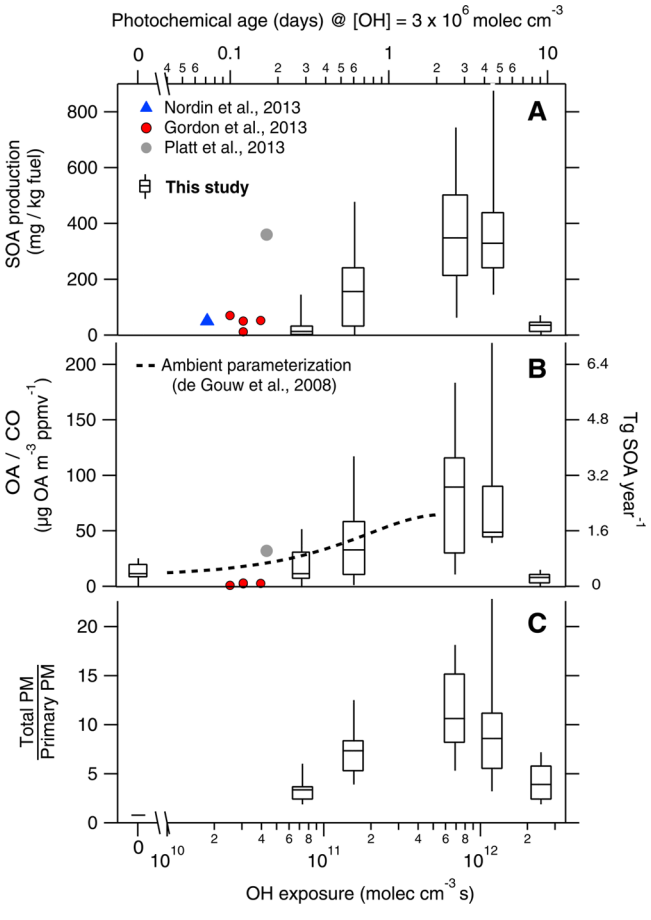

Figure 2. Box-and-whisker plots of SOA production as (a) fuel-based emission factors and (b) ΔOA/ΔCO enhancement ratios. Panel (c) shows total PM mass enhancement including inorganic species and BC. The symbols in (a) and (b) are SOA production data from published gasoline vehicle smog chamber studies.[13,32,33] Panel (b) shows the parametrization of ΔOA/ΔCO from de Gouw et al.[6] Sample size for each box-and-whisker plot was n = 11.

Results from smog chamber SOA formation studies performed with individual light-duty gasoline vehicles (LDGVs)[5−7] are also plotted in Figure 2. Comparisons can only be made at the lowest OH exposure given the limited oxidation in the smog chamber studies. SOA production measured by Nordin et al.[6] and Gordon et al.[5] are similar to the low OH exposure PAM reactor data. However, the Platt et al.[7] data shows a much larger mass enhancement at a comparable OH exposure (about an order of magnitude larger on a fuel-basis; Figure 2a). This may be because the Platt et al.[7] data are based on two experiments with a single LDV, and may not be representative of a broader range of vehicles and operating conditions.

Figure 2 suggests that the published smog chamber studies (except for Platt et al.[7]) may underestimate the ultimate SOA production from vehicle emissions due to limited OH exposure. The peak SOA production measured in the PAM reactor was about 10 times greater than that measured at low OH exposure in the smog chamber.

Field studies often characterize the SOA production downwind of urban areas using the ratio of background-corrected OA (ΔOA) to background-corrected CO (ΔCO) to account for the effects of dilution on OA levels.[11] Figure 2b plots ΔOA/ΔCO measured in the PAM reactor as a function of OH exposure. The agreement between the PAM reactor ΔOA/ΔCO ratio and the Platt et al.[7] chamber data suggests that the Platt et al.[7] vehicle may have had high VOC and CO emissions. Figure 2b also compares the PAM reactor data to the ΔOA/ΔCO from the parametrization of de Gouw et al. which was derived from aircraft measurements made downwind of urban areas in the northeastern United States.[10] The peak ΔOA/ΔCO measured in the tunnel occurs at the same OH exposure at which ambient ΔOA/ΔCO levels off in the de Gouw et al. parametrization.[10] In addition, the median ΔOA/ΔCO measured in the tunnel is very similar to the de Gouw et al. parametrization (±30% at higher OH exposures). Since as much as 90% of CO emissions in and downwind of urban areas are from motor vehicle exhaust,[40] this suggests that gas-phase oxidation of vehicle emissions may explain a large fraction of SOA production downwind of urban areas.

Figure 2c presents total PM mass enhancements, defined as the ratio of total PM mass measured downstream of the PAM reactor to that measured in the bypass line (primary PM mass). The PM mass is the sum of the species measured by the ACSM mass plus BC measured by the Aethalometer. The peak PM mass enhancement was ∼11 (10 times more secondary PM mass than primary PM emissions) after 2.7 OH days, demonstrating that the contribution of motor vehicle exhaust to ambient PM is dominated by secondary aerosol production.

3.3. SOA Composition. The ACSM mass spectra indicate that the chemical evolution of the organic aerosol inside the PAM reactor is similar to that observed in the atmosphere. Sample mass spectra at various levels of OH-exposure are presented in SI Figure S8. Figure 3 plots the correlation coefficient (r^2) between OA mass spectra as a function of OH exposure and published PMF factors derived from ambient measurements.[41,42] Unoxidized tunnel OA closely resembled the hydrocarbon-like OA factor (HOA; $r^2 > 0.9$) with the characteristic "picket fence" associated with the electronic impact ionization of alkyl chains (SI Figure S8).[43] Oxidation in the PAM reactor caused substantial growth in the m/z 44 (CO_2^+) signal, which is associated with organic acids.[44] After a few hours of equivalent atmospheric oxidation in the PAM reactor, the OA spectra most closely resembled semivolatile oxygenated OA factor (SV-OOA; $r^2 = 0.8$) but also resembled HOA factor ($r^2 = 0.75$) and low-volatility oxygenated OA factor ($r^2 = 0.65$). At higher OH exposures, the ACSM OA mass spectra most resembled LV-OOA factor ($r^2 = 0.9$). These trends in the ACSM mass spectra mirror the evolution of OA downwind of urban areas[12] and laboratory studies.[12,45,46]

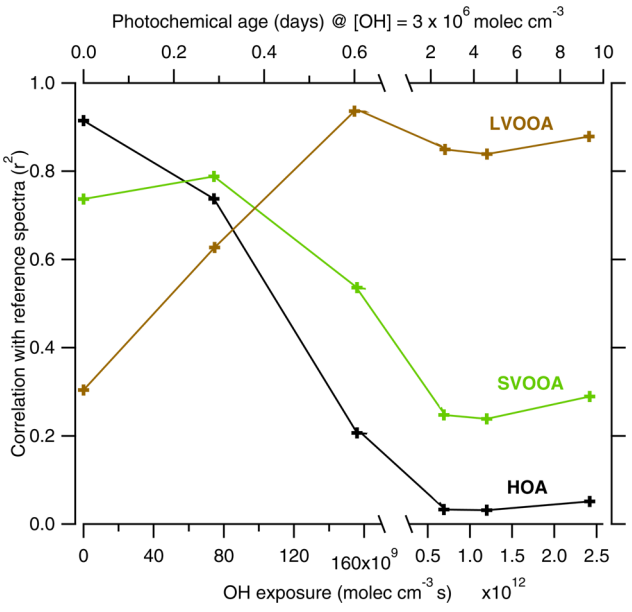

Figure 3. Correlation coefficients (r^2) between the ACSM mass spectra (this study) and published ambient PMF factors[41] as a function of OH exposure. These are data from a typical experiment (Evening rush hour: May 10th, 2013).

3.4. SOA Modeling. Comprehensive organic speciation was performed on the WAS and Tenax samples to better understand the SOA formation. These data are summarized in SI Table S3. They include concentrations of 72 individual organics, including single ring aromatics, polycyclic aromatic hydrocarbons (PAHs), alkanes, and alkenes. The emission rates of these species are comparable to recent dynamometer data (SI). A large fraction of the IVOC collected on the Tenax sorbent could not be speciated and therefore was classified as an unresolved complex mixture (UCM). The mass of the UCM was quantified using surrogate standards, as described in the online supplemental.

An effective SOA yield can be defined as the ratio of the measured SOA mass to measured gas-phase organic concentration (median speciated organics plus IVOC UCM). Using the median SOA production measured at each OH exposure, this ratio ranged from 8% at 0.3 OH days to 61% at 2.7 OH days. Therefore, the maximum effective SOA yield inside the PAM was 61% (23−78%, respectively, for 25th to 75th percentiles at 2.7 OH days), which is higher than yields measured in typical single compound smog chamber experiments. However, 2.7 OH days is a much higher oxidant exposure than in typical chamber experiments. Therefore, the very high effective yields measured at 2.7 OH days are likely due, in part, to multigenerational chemistry. In addition, there are likely SOA precursors that were not quantified, such as evaporated POA and other higher molecular weight species.[33] The effective yields at lower OH exposures are more consistent with published smog chamber data.

We also compared the measured SOA formation to predictions of an SOA model. SOA production was modeled as a two-step process. First-generation SOA from speciated precursors was calculated using the SOA module from the community multiscale air quality (CMAQ) model.[51] Briefly, precursors react to form semivolatile products derived from fitting smog chamber data. The gas-particle partitioning is described as a pseudoideal solution at equilibrium. Species lumping was based on the SAPRC mechanisms (see SI). To account for alkanes with varying carbon numbers and structures (linear, branched and cyclic), we used the scheme in Pye and Pouliot[52] to determine *n*-dodecane equivalent emissions. PAHs were lumped and modeled to form SOA using the surrogate naphthalene.[52] The model also accounts for unspeciated precursors, including the IVOC UCM measured with the Tenax sorbent and organic vapors associated with the semivolatile POA.[49] The mass concentrations of these vapors were estimated using the measured POA in the bypass line and the volatility distribution for gasoline exhaust of May et al.[50] First-generation SOA production from the POA vapors and the IVOC UCM were modeled as a *n*-tridecane (with a reaction rate constant of 1.51×10^{-11} cm^3 molecules^{-1} s^{-1}).[47]

The second step of the SOA model was to simulate the effects of multigenerational processing using the 2-D volatility basis set (2D-VBS). The first generation products were mapped on the 2D-VBS using the approach of Murphy et al.[48] and their chemical evolution was modeled using the parametrization for α-pinene from Donahue et al.[54]

Figure 4 presents the results from the SOA modeling. Speciated SOA precursors (single-ring aromatics, *n*-alkanes, and PAHs) undergoing a single generation of oxidation only explained about 20% of the median measured SOA after 2.7 OH days. Including SOA formation from unspeciated organics (POA vapors and IVOC UCM) tripled the predicted SOA mass, with predicted SOA accounting for about 65% of the OA after 2.7 OH days (short-dashed line in Figure 4). Therefore, unspeciated organics are predicted to contribute twice as much SOA as traditional, speciated precursors.

Figure 4 indicates that the model does not reproduce the magnitude nor timing of the peak SOA production. There are several possible explanations for the underprediction of the peak SOA mass production. The SOA yields in the model were derived from smog chamber experiments, which may underestimate SOA yields by as much as a factor of 4.[49] The model may not include all SOA precursors. Finally, the model may underpredict multigenerational SOA production. The 2D-VBS parametrizes the branching between the functionalization and fragmentation as a function of the O:C ratio. However, the O:C ratio of the first generation gas phase products was not

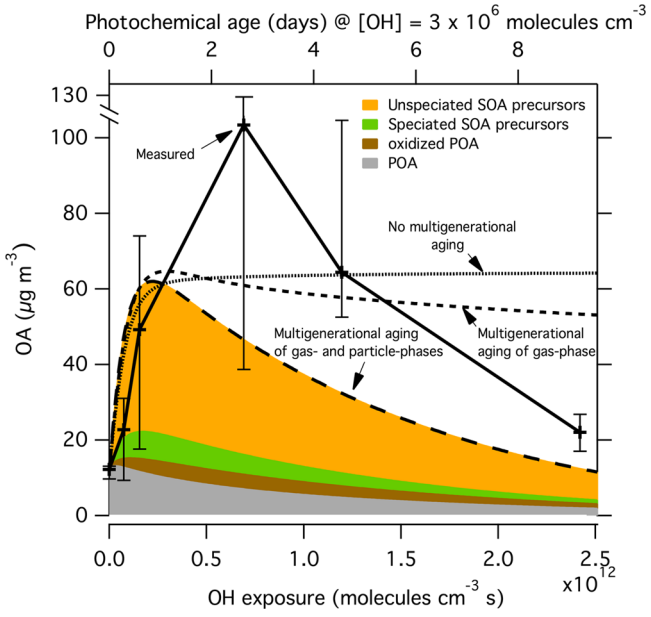

Figure 4. Model-measurement comparison. Measured data (median OA concentrations) are indicated by + symbols, with error bars representing 25th and 75th percentiles. The short-dashed line shows predicted SOA concentration from a single generation of gas-phase oxidation of speciated and unspeciated SOA precursors. The medium-dashed line show predicted SOA formed from speciated and unspeciated SOA precursors undergoing multigenerational processing in the gas-phase. The long-dashed line shows predicted SOA formed from speciated and unspeciated SOA precursors undergoing multigenerational processing in the gas- and particle-phases. The colored wedges are the individual contributions from each class of SOA precursor to SOA from gas- and particle-phase multigenerational processing (long-dashed line).

measured. It was assumed to be 0.4 based on Murphy et al.,[48] which is based on results from α-pinene experiments.[50] At an O:C ratio of 0.4, the 2D-VBS predicts that fragmentation reactions are dominant. If the O:C ratio of the first generation gas-phase products of vehicle exhaust are less than 0.4, then the 2D-VBS would predict substantial multigenerational SOA production.

In order to explain the fall off of the SOA production at high OH exposure, we had to include heterogeneous oxidation of OA with OH in the model (assuming an uptake coefficient of 1 or 2×10^{-12} cm^3 molecules^{-1} s^{-1}; long-dashed line in Figure 4). The distribution of functionalized and fragmented products from the heterogeneous reactions were assumed to be the same as those from gas-phase oxidation.[51] Therefore, heterogeneous reactions appear to be an important loss process for highly oxygenated OA in the PAM reactor.

Figure 4 also indicates that the model does not reproduce the timing of the peak SOA production. It predicts that the peak production occurs at lower OH exposures, equivalent to 1 day of atmospheric aging. This may be due to the model assuming instantaneous equilibrium gas/particle partitioning. The reaction time scales and residence time inside the PAM reactor (<100 s) are likely shorter than the partitioning time scales (order of minutes); therefore, instantaneous equilibrium may not be a good assumption and should be explored in future studies.

Although the model predictions do not perfectly reproduce the measured data, three key conclusions arise from these model simulations: (1) speciated SOA precursors (single-ring aromatics, PAHs, and alkanes) only explain a small fraction of the SOA formation from vehicle emissions, (2) unspeciated SOA precursors (i.e., UCM) contribute largest portion of predicted SOA, suggesting that unspeciated precursors are the dominant source of SOA in vehicle emissions consistent with Gordon et al.,[5] and (3) multigenerational processing of both gases and particles is necessary to explain SOA at longer time scales.

4. ATMOSPHERIC IMPLICATIONS

The SOA data can be scaled to estimate potential SOA production from mobile emissions in the United States. This estimate is defined as the product of the peak measured ΔOA/ΔCO in Figure 2b (median ~90 μg m^{-3} ppmv^{-1} at 2.7 OH days) and the U.S. mobile source CO emission taken from the National Emission Inventory (NEI; 37.3 Tg CO year^{-1}).[52] The NEI attributes 90% of CO emissions in the United States to mobile sources—on- and off-road gasoline vehicles.

We estimate SOA production of 2.9 $\pm$ 1.6 Tg yr^{-1} in the United States from mobile source emissions. This estimate is somewhat higher than previous estimates. Bahreini et al. (2012) estimated an SOA formation rate of ~1 Tg yr^{-1} in the U.S. from mobile gasoline sources; de Gouw et al.[53] calculated a production rate of 2.1 Tg SOA yr^{-1} from urban VOCs. Figure 2 indicates that the measured SOA production also agreed well with the parametrization of de Gouw et al.,[10] supporting the conclusion that mobile source emissions contribute a large fraction of anthropogenic SOA downwind of urban areas.

The PAM reactor data also underscore that the contribution of on-road vehicle exhaust to ambient PM exposure in the United States is likely driven by secondary aerosol production, not primary PM emissions. The estimated SOA production from mobile source emissions is six times higher than the NEI estimate of primary PM emissions from these sources. Furthermore, mobile source NO_X emissions contribute significantly to secondary nitrate formation. This highlights the importance of controlling aerosol precursors in on-road vehicle emissions.

■ ASSOCIATED CONTENT

Supporting Information

Additional information as noted in the text. This material is available free of charge via the Internet at http://pubs.acs.org.

■ AUTHOR INFORMATION

Notes

The authors declare no competing financial interest.

■ ACKNOWLEDGMENTS

We thank the Pennsylvania Department of Transportation (PennDOT) for granting us access to the Fort Pitt Tunnel. This article was developed under a STAR Research Assistance Agreement No. RD834554 awarded by the U.S. Environmental Protection Agency. It has not been formally reviewed by the EPA. The views expressed in this document are solely those of authors and the EPA does not endorse any products or commercial services mentioned in this publication. D.S.T. recognizes P. J. Adams, N.M. Donahue, and E.S. Robinson (CMU) for helpful discussions. A.T.L. acknowledges J. L. Jimenez (UC Colorado), T.B. Onasch (BC/ARI), D. R. Worsnop (ARI), W. H. Brune (PSU), and P. Davidovits

(BC) for helpful discussions and funding from the National Science Foundation grant No. AGS-1244918 and the Office of Science, Office of Science (BER), Department of Energy (Atmospheric Science Program) grants No. DE-SC0006980 and DE-FG02-05ER63995 to Boston College and Aerodyne Research, Inc.

REFERENCES

(1) Fine, P. M.; Shen, S.; Sioutas, C. Inferring the sources of fine and ultrafine particulate matter at downwind receptor sites in the Los Angeles basin using multiple continuous measurements. Special issue of Aerosol Science and Technology on findings from the fine particulate matter supersites program. *Aerosol Sci. Technol.* **2004**, *38*, 182−195.

(2) Zhang, Q.; Stanier, C. O.; Canagaratna, M. R.; Jayne, J. T.; Worsnop, D. R.; Pandis, S. N.; Jimenez, J. L. Insights into the chemistry of new particle formation and growth events in Pittsburgh based on aerosol mass spectrometry. *Environ. Sci. Technol.* **2004**, *38*, 4797−4809.

(3) Twomey, S. Pollution and the planetary albedo. *Atmos. Environ.* **1974**, *8*, 1251−1256.

(4) Dockery, D. W.; Pope, C. A., III Health effects of fine particulate air pollution: Lines that connect. *J. Air Waste Manage. Assoc.* **2006**, *56*, 709+.

(5) Gordon, T. D.; Presto, A. A.; May, A. A.; Nguyen, N. T.; Lipsky, E. M.; Donahue, N. M.; Gutierrez, A.; Zhang, M.; Maddox, C.; Rieger, P.; et al. Secondary organic aerosol formation exceeds primary particulate matter emissions for light-duty gasoline vehicles. *Atmos. Chem. Phys. Discuss.* **2013**, *13*, 23173−23216.

(6) Nordin, E. Z.; Eriksson, A. C.; Roldin, P.; Nilsson, P. T.; Carlsson, J. E.; Kajos, M. K.; Hellén, H.; Wittbom, C.; Rissler, J.; Löndahl, J.; et al. Secondary organic aerosol formation from idling gasoline passenger vehicle emissions investigated in a smog chamber. *Atmos. Chem. Phys.* **2013**, *13*, 6101−6116.

(7) Platt, S. M.; El Haddad, I.; Zardini, A. A.; Clairotte, M.; Astorga, C.; Wolf, R.; Slowik, J. G.; Temime-Roussel, B.; Marchand, N.; Ježek, I.; et al. Secondary organic aerosol formation from gasoline vehicle emissions in a new mobile environmental reaction chamber. *Atmos. Chem. Phys.* **2013**, *13*, 9141−9158.

(8) Chirico, R.; DeCarlo, P. F.; Heringa, M. F.; Tritscher, T.; Richter, R.; Prévôt, A. S. H.; Dommen, J.; Weingartner, E.; Wehrle, G.; Gysel, M.; et al. Impact of aftertreatment devices on primary emissions and secondary organic aerosol formation potential from in-use diesel vehicles: Results from smog chamber experiments. *Atmos. Chem. Phys.* **2010**, *10*, 11545−11563.

(9) Volkamer, R.; Jimenez, J. L.; San Martini, F.; Dzepina, K.; Zhang, Q.; Salcedo, D.; Molina, L. T.; Worsnop, D. R.; Molina, M. J. Secondary organic aerosol formation from anthropogenic air pollution: Rapid and higher than expected. *Geophys. Res. Lett.* **2006**, *33*, L17811.

(10) De Gouw, J. A.; Brock, C. A.; Atlas, E. L.; Bates, T. S.; Fehsenfeld, F. C.; Goldan, P. D.; Holloway, J. S.; Kuster, W. C.; Lerner, B. M.; Matthew, B. M.; et al. Sources of particulate matter in the northeastern United States in summer: 1. Direct emissions and secondary formation of organic matter in urban plumes. *J. Geophys. Res. Atmos.* **2008**, *113*, D08301.

(11) De Gouw, J.; Jimenez, J. L. Organic aerosols in the earth's atmosphere. *Environ. Sci. Technol.* **2009**, *43*, 7614−7618.

(12) Jimenez, J. L.; Canagaratna, M. R.; Donahue, N. M.; Prevot, A. S. H.; Zhang, Q.; Kroll, J. H.; DeCarlo, P. F.; Allan, J. D.; Coe, H.; Ng, N. L.; et al. Evolution of organic aerosols in the atmosphere. *Science* **2009**, *326*, 1525−1529.

(13) Heringa, M. F.; DeCarlo, P. F.; Chirico, R.; Tritscher, T.; Dommen, J.; Weingartner, E.; Richter, R.; Wehrle, G.; Prévôt, A. S. H.; Baltensperger, U. Investigations of primary and secondary particulate matter of different wood combustion appliances with a high-resolution time-of-flight aerosol mass spectrometer. *Atmos. Chem. Phys.* **2011**, *11*, 5945−5957.

(14) Heringa, M. F.; DeCarlo, P. F.; Chirico, R.; Tritscher, T.; Clairotte, M.; Mohr, C.; Crippa, M.; Slowik, J. G.; Pfaffenberger, L.; Dommen, J.; et al. A new method to discriminate secondary organic aerosols from different sources using high-resolution aerosol mass spectra. *Atmos. Chem. Phys.* **2012**, *12*, 2189−2203.

(15) Gordon, T. D. .; Tkacik, D. S. .; Presto, A. A. .; Zhang, M. .; Jathar, S. H. .; Nguyen, N. T. .; Massetti, J. .; Truong, T. .; Cicero-Fernandez, P. .; Maddox, C. .; et al. Primary gas- and particle-phase emissions and secondary organic aerosol production from gasoline and diesel off-road engines. *Environ. Sci. Technol.* **2013**, *47*, 14137−14146.

(16) Lambe, A. T.; Onasch, T. B.; Croasdale, D. R.; Wright, J. P.; Martin, A. T.; Franklin, J. P.; Massoli, P.; Kroll, J. H.; Canagaratna, M. R.; Brune, W. H.; et al. Transitions from functionalization to fragmentation reactions of laboratory secondary organic aerosol (SOA) generated from the OH oxidation of alkane precursors. *Environ. Sci. Technol.* **2012**, *46*, 5430−5437.

(17) Fraser, M. P.; Cass, G. R. Detection of excess ammonia emissions from in-use vehicles and the implications for fine particle control. *Environ. Sci. Technol.* **1998**, *32*, 1053−1057.

(18) Grieshop, A. P.; Lipsky, E. M.; Pekney, N. J.; Takahama, S.; Robinson, A. L. Fine particle emission factors from vehicles in a highway tunnel: Effects of fleet composition and season. *Atmos. Environ.* **2006**, *40* (Supple), 287−298.

(19) Chirico, R.; Prevot, A. S. H.; DeCarlo, P. F.; Heringa, M. F.; Richter, R.; Weingartner, E.; Baltensperger, U. Aerosol and trace gas vehicle emission factors measured in a tunnel using an aerosol mass spectrometer and other on-line instrumentation. *Atmos. Environ.* **2011**, *45*, 2182−2192.

(20) Kang, E.; Root, M. J.; Toohey, D. W.; Brune, W. H. Introducing the concept of potential aerosol mass (PAM). *Atmos. Chem. Phys.* **2007**, *7*, 5727−5744.

(21) EIA. *Residential Transportation Energy Consumption Survey*; U.S. Energy Information Administration, 1994.

(22) Schauer, J. J.; Kleeman, M. J.; Cass, G. R.; Simoneit, B. R. T. Measurement of emissions from air pollution sources. 5. C1−C32 organic compounds from gasoline-powered motor vehicles. *Environ. Sci. Technol.* **2002**, *36*, 1169−1180.

(23) Loza, C. L.; Craven, J. S.; Yee, L. D.; Coggon, M. M.; Schwantes, R. H.; Shiraiwa, M.; Zhang, X.; Schilling, K. A.; Ng, N. L.; Canagaratna, M. R.; et al. Secondary organic aerosol yields of 12-carbon alkanes. *Atmos. Chem. Phys.* **2014**, *14*, 1423−1439.

(24) Kanaya, Y.; Cao, R.; Akimoto, H.; Fukuda, M.; Komazaki, Y.; Yokouchi, Y.; Koike, M.; Tanimoto, H.; Takegawa, N.; Kondo, Y. Urban photochemistry in central Tokyo: 1. Observed and modeled OH and HO_2 radical concentrations during the winter and summer of 2004. *J. Geophys. Res., Atmos.* **2007**, *112*, D21312.

(25) Ng, N. L.; Herndon, S. C.; Trimborn, A.; Canagaratna, M. R.; Croteau, P. L.; Onasch, T. B.; Sueper, D.; Worsnop, D. R.; Zhang, Q.; Sun, Y. L.; et al. An aerosol chemical speciation monitor (ACSM) for routine monitoring of the composition and mass concentrations of ambient aerosol. *Aerosol Sci. Technol.* **2011**, *45*, 780−794.

(26) Docherty, K. S.; Jaoui, M.; Corse, E.; Jimenez, J. L.; Offenberg, J. H.; Lewandowski, M.; Kleindienst, T. E. Collection efficiency of the aerosol mass spectrometer for chamber-generated secondary organic aerosols. *Aerosol Sci. Technol.* **2012**, *47*, 294−309.

(27) Saukko, E.; Lambe, A. T.; Massoli, P.; Koop, T.; Wright, J. P.; Croasdale, D. R.; Pedernera, D. A.; Onasch, T. B.; Laaksonen, A.; Davidovits, P.; et al. Humidity-dependent phase state of SOA particles from biogenic and anthropogenic precursors. *Atmos. Chem. Phys.* **2012**, *12*, 7517−7529.

(28) Middlebrook, A. M.; Bahreini, R.; Jimenez, J. L.; Canagaratna, M. R. Evaluation of composition-dependent collection efficiencies for the aerodyne aerosol mass spectrometer using field data. *Aerosol Sci. Technol.* **2011**, *46*, 258−271.

(29) Presto, A. A.; Miracolo, M. A.; Donahue, N. M.; Robinson, A. L. Secondary organic aerosol formation from high-NO_x photo-oxidation of low volatility precursors: *n*-Alkanes. *Environ. Sci. Technol.* **2010**, *44*, 2029−2034.

(30) Simpson, I. J.; Colman, J. J.; Swanson, A. L.; Bandy, A. R.; Thornton, D. C.; Blake, D. R.; Rowland, F. S. Aircraft measurements of dimethyl sulfide (DMS) using a whole air sampling technique. *J. Atmos. Chem.* **2001**, *39*, 191−213.
(31) Tang, W.; Raymond, T.; Wittig, B.; Davidson, C.; Pandis, S.; Robinson, A.; Crist, K. Spatial variations of $PM_{2.5}$ during the Pittsburgh air quality study. *Aerosol Sci. Technol.* **2004**, *38*, 80−90.
(32) Rees, S. L.; Robinson, A. L.; Khlystov, A.; Stanier, C. O.; Pandis, S. N. Mass balance closure and the Federal Reference Method for $PM_{2.5}$ in Pittsburgh, Pennsylvania. *Atmos. Environ.* **2004**, *38*, 3305−3318.
(33) May, A. A.; Presto, A. A.; Hennigan, C. J.; Nguyen, N. T.; Gordon, T. D.; Robinson, A. L. Gas-particle partitioning of primary organic aerosol emissions: (1) Gasoline vehicle exhaust. *Atmos. Environ.* **2013**, *77*, 128−139.
(34) Gordon, T. D.; Presto, A. A.; Nguyen, N. T.; Robertson, W. H.; Na, K.; Sahay, K. N.; Zhang, M.; Maddox, C.; Rieger, P.; Chattopadhyay, S.; et al. Secondary organic aerosol production from diesel vehicle exhaust: impact of aftertreatment, fuel chemistry and driving cycle. *Atmos. Chem. Phys. Discuss.* **2013**, *13*, 24223−24262.
(35) May, A. A.; Nguyen, N. T.; Presto, A. A.; Gordon, T. D.; Lipsky, E. M.; Karve, M.; Gutierrez, A.; Robertson, W. H.; Zhang, M.; Brandow, C.; et al. Gas- and particle-phase primary emissions from in-use, on-road gasoline and diesel vehicles. *Atmos. Environ.* **2014**, *88*, 247−260.
(36) Durbin, T. D.; Wilson, R. D.; Norbeck, J. M.; Miller, J. W.; Huai, T.; Rhee, S. H. Estimates of the emission rates of ammonia from light-duty vehicles using standard chassis dynamometer test cycles. *Atmos. Environ.* **2002**, *36*, 1475−1482.
(37) Burgard, D. A.; Bishop, G. A.; Stedman, D. H. Remote sensing of ammonia and sulfur dioxide from on-road light duty vehicles. *Environ. Sci. Technol.* **2006**, *40*, 7018−7022.
(38) Kean, A. J.; Littlejohn, D.; Ban-Weiss, G. A.; Harley, R. A.; Kirchstetter, T. W.; Lunden, M. M. Trends in on-road vehicle emissions of ammonia. *Atmos. Environ.* **2009**, *43*, 1565−1570.
(39) Mysliwiec, M. J.; Kleeman, M. J. Source apportionment of secondary airborne particulate matter in a polluted atmosphere. *Environ. Sci. Technol.* **2002**, *36*, 5376−5384.
(40) U. S. EPA. *National Air Quality and Emissions Trends Report—2003 Special Studies Edition*; Research Triangle Park, NC, 2003.
(41) Ng, N. L.; Canagaratna, M. R.; Jimenez, J. L.; Chhabra, P. S.; Seinfeld, J. H.; Worsnop, D. R. Changes in organic aerosol composition with aging inferred from aerosol mass spectra. *Atmos. Chem. Phys.* **2011**, *11*, 6465−6474.
(42) Ulbrich, I. M.; Canagaratna, M. R.; Zhang, Q.; Worsnop, D. R.; Jimenez, J. L. Interpretation of organic components from positive matrix factorization of aerosol mass spectrometric data. *Atmos. Chem. Phys.* **2009**, *9*, 2891−2918.
(43) Canagaratna, M. R.; Jayne, J. T.; Ghertner, D. A.; Herndon, S.; Shi, Q.; Jimenez, J. L.; Silva, P. J.; Williams, P.; Lanni, T.; Drewnick, F.; et al. Chase studies of particulate emissions from in-use New York City Vehicles. *Aerosol Sci. Technol.* **2004**, *38*, 555−573.
(44) Aiken, A. C.; DeCarlo, P. F.; Kroll, J. H.; Worsnop, D. R.; Huffman, J. A.; Docherty, K. S.; Ulbrich, I. M.; Mohr, C.; Kimmel, J. R.; Sueper, D.; et al. O/C and OM/OC ratios of primary, secondary, and ambient organic aerosols with high-resolution time-of-flight aerosol mass spectrometry. *Environ. Sci. Technol.* **2008**, *42*, 4478−4485.
(45) Grieshop, A. P.; Donahue, N. M.; Robinson, A. L. Laboratory investigation of photochemical oxidation of organic aerosol from wood fires 2: analysis of aerosol mass spectrometer data. *Atmos. Chem. Phys.* **2009**, *9*, 2227−2240.
(46) Lambe, A. T.; Onasch, T. B.; Massoli, P.; Croasdale, D. R.; Wright, J. P.; Ahern, A. T.; Williams, L. R.; Worsnop, D. R.; Brune, W. H.; Davidovits, P. Laboratory studies of the chemical composition and cloud condensation nuclei (CCN) activity of secondary organic aerosol (SOA) and oxidized primary organic aerosol (OPOA). *Atmos. Chem. Phys.* **2011**, *11*, 8913−8928.
(47) Jathar, S. H.; Gordon, T. D.; Hennigan, C. J.; Pye, H. O. T.; Donahue, N. M.; Adams, P. J.; Robinson, A. L. Unspeciated organic emissions from combustion sources and their influence on the secondary organic aerosol budget in the United States. *Proc. Natl. Acad. Sci. U. S. A.* **2014**, *111*, 10473−10478.
(48) Murphy, B. N.; Donahue, N. M.; Fountoukis, C.; Pandis, S. N. Simulating the oxygen content of ambient organic aerosol with the 2D volatility basis set. *Atmos. Chem. Phys.* **2011**, *11*, 7859−7873.
(49) Zhang, X.; Cappa, C. D.; Jathar, S. H.; McVay, R. C.; Ensberg, J. J.; Kleeman, M. J.; Seinfeld, J. H. Influence of vapor wall loss in laboratory chambers on yields of secondary organic aerosol. *Proc. Natl. Acad. Sci. U. S. A.* **2014**, *111*, 5802−5807.
(50) Donahue, N. M.; Epstein, S. A.; Pandis, S. N.; Robinson, A. L. A two-dimensional volatility basis set: 1. Organic-aerosol mixing thermodynamics. *Atmos. Chem. Phys.* **2011**, *11*, 3303−3318.
(51) Smith, J. D.; Kroll, J. H.; Cappa, C. D.; Che, D. L.; Liu, C. L.; Ahmed, M.; Leone, S. R.; Worsnop, D. R.; Wilson, K. R. The heterogeneous reaction of hydroxyl radicals with sub-micron squalane particles: A model system for understanding the oxidative aging of ambient aerosols. *Atmos. Chem. Phys.* **2009**, *9*, 3209−3222.
(52) U. S. EPA *2008 National Emissions Inventory version 3*, 2013.
(53) De Gouw, J. A.; Middlebrook, A. M.; Warneke, C.; Goldan, P. D.; Kuster, W. C.; Roberts, J. M.; Fehsenfeld, F. C.; Worsnop, D. R.; Canagaratna, M. R.; Pszenny, A. A. P.; et al. Budget of organic carbon in a polluted atmosphere: Results from the New England Air Quality Study in 2002. *J. Geophys. Res.* **2005**, *110*, D16305.